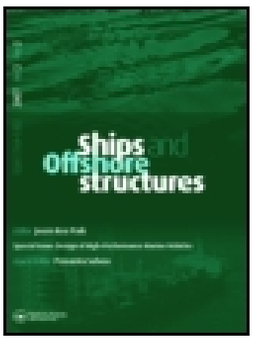

Ships and Offshore Structures

ISSN: 1744-5302 (Print) 1754-212X (Online) Journal homepage: http://www.tandfonline.com/loi/tsos20

Statistical assessment of seismic fragility curves for steel jacket platforms considering global dynamic instability

M. Abyani, B. Asgarian & M. Zarrin

To cite this article: M. Abyani, B. Asgarian & M. Zarrin (2017): Statistical assessment of seismic fragility curves for steel jacket platforms considering global dynamic instability, Ships and Offshore Structures, DOI: 10.1080/17445302.2017.1386078

To link to this article: http://dx.doi.org/10.1080/17445302.2017.1386078

Published online: 23 Oct 2017.

SHIPS AND OFFSHORE STRUCTURES, 2017
https://doi.org/10.1080/17445302.2017.1386078

Taylor & Francis
Taylor & Francis Group

Statistical assessment of seismic fragility curves for steel jacket platforms considering global dynamic instability

M. Abyani, B. Asgarian and M. Zarrin

Faculty of Civil Engineering, K. N. Toosi University of Technology, Tehran, Iran

ABSTRACT

Many probabilistic studies in the field of offshore structures assume that the drift demand distributes lognormally around its median at all the intensity levels. However, this assumption may not be formally validated, and the purpose of this study is to investigate the assumption of lognormal distribution of the drift demand for the fixed offshore platforms, using Anderson–Darling goodness of fit test. The lognormal hypothesis for the drift demand can be investigated at two different regions as: (1) low intensity levels without any collapse case and (2) higher intensity levels with collapse cases. To this end, both the sample median and sample geometric mean are considered as the estimators of lognormal central tendency. The results indicate that the lognormal hypothesise is accepted based on the sample geometric mean at all the intensity levels. Nevertheless, the lognormal hypothesise is rejected at some intensity levels if the sample median is the central estimator.

ARTICLE HISTORY
Received 1 July 2017
Accepted 4 September 2017

KEYWORDS
Incremental dynamic analysis; seismic; fragility; offshore; jacket platform

1. Introduction

Earthquake is one of the most destructive natural disasters which may make drastic damages to the existing structures. Different random nature of earthquake such as occurrence time and location or seismic wave propagation makes it quite complicated for the engineers to anticipate the exact seismic behaviour of the structures. However, after the 1994 Northridge and the 1995 Kobe earthquakes, significant progress was made in earthquake engineering by Federal Management Agency (FEMA) and SAC (joint venture of Structural Engineers Association of California (SEA), Applied Technology Council (ATC), Consortium of Universities for Research in Earthquake Engineering (CUREE)) projects. This highly efficient project has been proposed in FEMA-350/351 guidelines (SAC/ FEMA-2000a, 2000b).

The analytical framework of seismic reliability evaluation has been widely expanded by Jalayer and Cornell (Cornell et al. 2002; Jalayer 2003). They derived closed form expressions for the probability of exceeding a limit state considering both aleatoric and epistemic uncertainties in structural and seismic Analyses. This framework became more simplified in a Demand and Capacity Factored Design (DCFD) format (Cornell et al. 2002; Jalayer 2003) which is quite similar to the familiar Load and Resistance Factor Design (LRFD) format (AISC 2003). This format makes it possible to calculate the seismic reliability of the structure at each selected confidence level.

In this process, one of the most fundamental assumptions introduced by Shome (1999) is that the maximum interstory drift ratio (MIDR) distributes lognormally at each level of spectral acceleration. It could be easily proven that for a perfectly lognormal random variable (a lognormal population with infinite sample size), the mean of the logarithm of that variable is equal to the logarithm of the median of the same variable (Benjamin and Cornell 1970; Soong 2004). As a result, MIDR demand distributes lognormally around its median at each level of spectral acceleration (S_a) (Shome 1999). However, in a lognormal sample with a finite sample size, the logarithm of the sample median is not exactly equal to the mean of the logarithm of the same sample, and consequently, the mentioned assumption might have some approximations. On the contrary, for any arbitrary random variable the sample geometric mean exactly equals the mean of the logarithm of that sample (Shih and Binkowitz 1967). In this respect, Abyani et al. (2017) compared the analytical framework of seismic reliability evaluation of steel moment frames based on the sample median and the sample geometric mean as the index of central tendency. The results of their study illustrated that the sample geometric mean could lead to more accurate results.

From another perspective, in the last two decades, a lot of effort has been made to evaluate and improve the performance-based assessments of the jacket type offshore platforms (JTOPs) (Hasan et al. 2010; Jahanmard et al. 2015; Elsayed et al. 2016). In 1996, Det Norske Veritas (DNV 1996) published a guideline report for the offshore structural reliability which comprised experience and knowledge on the application of probabilistic methods to structural design and provided advice on probabilistic modelling and structural reliability analysis of jacket structures. In another study by Jahanmard et al. (2015), wave endurance time (WET) was addressed as an applicable method for performance-based evaluation of fixed offshore platforms under extreme waves. In this research, artificial wave records called wave functions were designed so that their excitations gradually increase with time. Consequently, the main advantage of this approach was that it could assess the structural performance under various wave load conditions through a single time-history analysis. Elsayed et al. (2016) presented a new method for reliability assessment of a fixed offshore jacket

CONTACT M. Zarrin mo_zarrin@yahoo.com

platform against earthquake collapse. They computed the probability of platform collapse under seismic loading using a finite element reliability code. The first and second order reliability methods were used to calculate the safety indices, which could be compared with the target safety levels in offshore platform design codes.

Additionally, uncertainty modelling with the nonlinear dynamic analysis of JTOPs was discussed for how to account for the different uncertainties in the reliability assessments. Since jacket platforms may have inelastic behaviour during strong ground motions, it is necessary to use advanced structural analysis methods such as incremental dynamic analysis (IDA) (Vamvatsikos and Cornell 2002). Asgarian and Ajamy (2010) studied the seismic performance of the JTOPs, employing IDA for the structural analysis. They used the story drift as the engineering demand parameter (EDP) and first mode-spectral acceleration as the intensity measure (IM). Golafshani et al. (2011) proposed the method of probabilistic incremental wave analysis (PIWA) to evaluate the performance of JTOPs subjecting to sever wave loadings. In this approach, both static and dynamic wave analyses were implemented to estimate the distribution of wave height intensities. Also, an efficient combination of Latin hypercube sampling (LHS) (McKay et al. 1979) and simulated annealing (SA) technique (Vorechovsky and Novak 2009) was employed to reduce the amount of computational expenses. Further, Ajamy et al. (2014) introduced a comprehensive interaction IDA method to incorporate different sources of uncertainties associated with seismic load, modelling parameters and soil properties in the stochastic seismic analysis of JTOPs. In order to propagate these uncertainties, they used the same combination of LHS and SA technique to model the correlation of the uncertain parameters such as yield strength, elasticity modulus, shear wave velocity, shear modulus reduction and damping ratio. In another study, El-Din and Kim (2014) developed a simple methodology for seismic life cycle cost (LCC) estimation of steel jacket platforms. They utilised equivalent single degree of freedom system instead of the main structure, and eliminated the full IDA and fragility analysis. Instead, approximate fragility curves and localised IDA curves were used as well as a probabilistic simple closed-form solution for loss estimation.

In all these studies (Asgarian and Ajamy 2010; Golafshani et al. 2011; Ajamy et al. 2014; El-Din and Kim 2014), it was assumed that the structural demand conditional on a seismic intensity or a wave height level follows a lognormal distribution around its sample median. However, this paper aims to investigate the validity of lognormal hypothesis for the structural demand of JTOP. In this regard, Anderson–Darling (AD) goodness of fit test (Anderson and Darling 1954) has been used to check whether the lognormal distribution is suitable for the structural demand of fixed offshore platforms or not. Furthermore, it is intended to compare the accuracy of seismic fragility curves based on both the sample median and the sample geometric mean as the statistical index of lognormal central tendency, in two regions: (1) where no records has reached the global dynamic instability and (2) at higher intensity levels where the records consecutively reach their collapse capacities.

2. Preliminary probabilistic considerations

This section aims to discuss some preliminary probabilistic subjects required for the evaluations of this study.

2.1. Central tendency in lognormal distribution

The probability density function of a lognormal random variable (f) is defined as (Soong 2004):

$$f(D;\mu,\sigma) = \frac{1}{D\sigma\sqrt{2\pi}} \exp\left(-\frac{(Ln(D)-\mu)^2}{2\sigma^2}\right) \quad (1)$$

where D is a lognormal random variable with the statistical properties equal to μ (the mean of the natural logarithm of the random variable D) and σ (the standard deviation of the natural logarithm of the random variable D).

It can be proved that for a perfectly lognormal random variable such as D (a lognormal population with infinite sample size), the natural logarithm of the median of D is equal to μ (Benjamin and Cornell 1970; Soong 2004). This is the reason why the sample median has been considered as the lognormal central tendency in many previous studies (Cornell et al. 2002; Jalayer 2003; Asgarian and Ajamy 2010; Golafshani et al. 2011; Vamvatsikos 2013; Ajamy et al. 2014; El-Din and Kim 2014). Nevertheless, the natural logarithm of the sample median of a lognormal random variable with a finite sample size is not equal to the mean of the natural logarithm of that sample. On the other hand, the natural logarithm of the sample geometric mean of any arbitrary random variable is always equal to the mean of the natural logarithm of the same sample, regardless of its sample size (Abyani et al. 2017). Hence, regarding the maximum likelihood estimation (MLE) method, the sample geometric mean is regarded as a more efficient estimator of lognormal central tendency (Walpole et al. 2002). In other words, for the lognormal variable D, the sample geometric mean is the MLE estimator and the sample median is the rank estimator of the exponential of μ(Shih and Binkowitz 1967).

2.2. Seismic fragility curves

Seismic fragility evaluation is the core of probabilistic safety assessments of structures, which can be expressed through a fragility curve. A fragility function demonstrates the conditional probability that the structural capacity fails to resist the structural demand, given the seismic intensity (Celik and Ellingwood 2010). Considering the IDA curves, the MIDR demand fragility can be assessed at each level of spectral acceleration S_a as the parameter of IM. In case the global dynamic instability is not happening at the given IM level, the analytical fragility function is calculated by the two parameter lognormal cumulative distribution function (CDF) (Shome 1999; Cornell et al. 2002; Jalayer 2003). Nonetheless, at higher IM levels where the ground motion records reach their collapse capacities, the three parameter distribution proposed by Shome (1999) is capable of estimating the distribution of the drift demand with cases of global dynamic instability. In fact, the analytical expression of the three parameter distribution has been derived based on the disaggregation of the demand response values into two groups: non-collapse (NC) and collapse groups. The mean of the natural

logarithm of the NC drift demands $d|NC, S_a$ at the given S_a level ($\mu(Ln(d|NC, S_a))$), the standard deviation of the natural logarithm of the NC drift demands at the given S_a level ($\beta_{d|NC,S_a} = \sigma(Ln(d|NC, S_a))$) and the probability of NC response values $P_{NC|S_a}$ at the given S_a level are the three parameters of this distribution function. It is noted that the probability of NC drift values at the given S_a level equals the ratio of the number of NC records to the number of all the records at the same S_a level (Shome 1999; Jalayer 2003), which is always less than or equal to unity.

$$F(d|S_a) = \Phi\left(\frac{\ln(d) - \mu(Ln(d|NC, S_a))}{\beta_{d|NC,S_a}}\right).P_{NC|S_a} \quad (2)$$

In this equation, Φ represents the standard normal CDF.

2.3. Anderson–Darling goodness of fit test

AD test can be regarded as a modification of the Cramer-Von Mises test, and is one of the most powerful goodness of fit tests (Anderson and Darling 1954) based on empirical distribution function (EDF). In fact, AD test was developed as an alternative to other statistical tests for detecting sample distributions' departure from normality (Engmann and Cousineau 2011). The AD test statistic (ST_{AD}) is categorised as the quadratic class of the EDF statistic which is based on the squared difference between the empirical CDF (ECDF) and the hypothesised analytical distribution F as Equation (3). For sample values sorted in ascending order of magnitude, denoted by $x_1, x_2, \ldots, x_n$ the ECDF of x_i is calculated by $\frac{i}{n}$, where i is the rank of x.

$$ST_{AD} = n\int_{-\infty}^{+\infty}[\mathrm{ECDF}(x) - F(x)]^2.\psi(F(x)).dF(x) \quad (3)$$

ST_{AD} is the average of the squared discrepancy $[\mathrm{ECDF}(x) - F(x)]^2$ weighted by $\psi(F(x))$, and ψ indicates a nonnegative weight function that could be derived from different expressions such as $\psi = [F(x)(1 - F(x)]^{-1}$. The AD test is more sensitive to deviations in the tails of the distributions (Anderson and Darling 1954), and is more powerful than the Kolmogorov–Smirnov (KS) test (Benjamin and Cornell 1970; Razali and Wah 2011).

3. Description of the case study platform

The considered sample platform is one of the two newly designed similar platforms located in the Persian Gulf. This platform was planned and designed in 2010 and was installed in 2012 in water depth of about 75 m. The platform comprises a four-leg jacket supporting a wellhead deck, which was designed and analysed in accordance with the requirements of the American Petroleum Institute (API RP2A-WSD 2007).

The steel jacket is composed of six horizontal plan frames that form an unbraced story and four braced stories, two vertical legs and two legs battered to 1:10 in direction y. The jacket is approximately 84 m high from mud line up to top of the jacket. The utilised lateral resisting systems of the jacket are the V-bracing and inverted V-bracing systems, which constitute a Multistory X-bracing system at the second and fourth horizontal plan framings (See Figure 1). The Jacket is fixed to the ground by four through leg piles. The gap between pile and leg is filled with grout to provide a composite section termed grouted section.

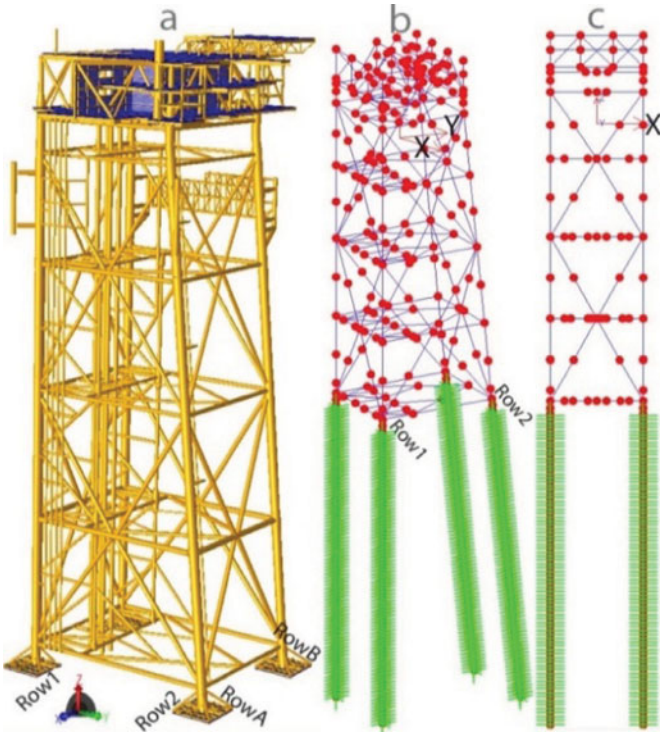

Figure 1. Perspective plot of the HE2 platform (a) 3D sacs model, (b) 3D openSEES model and (c) Row1 view. (This figure is available in colour online.)

All top side and jacket masses including structural and hydrodynamic masses have been considered as concentrated masses at the element joints. Accordingly, all top side and jacket loads are applied at joints as equivalent point loads.

During the design phase, a three-dimensional space frame computer model of the platform with all primary and secondary components were created by using the structural analysis computer system (SACS) suite (Figure 1(a)). Herein, a numerical model of the aforementioned sample platform has been developed using OpenSEES software (Mazzoni et al. 2007). The schematic configuration of the model created in OpenSEES is also demonstrated in Figure 2(b,c).

The soil profile was determined based on the results of a comprehensive geotechnical investigation including some boreholes and a piezocone penetration tests within the location of the project. The soil stratigraphy conditions disclosed by the borehole performed at the platform location are medium dense silty or clayey sand to around 2.0 m depth from mudline, followed by firm locally sandy clay to around 3.8 m. Firm becoming stiff clay, generally of intermediate to high plasticity was encountered to approximately 70 m followed by very stiff becoming hard clay of high plasticity to the completion depth of each borehole.

4. Numerical modelling procedures

In this paper, the nonlinear beam-column element (distributed plasticity) has been used to model the jacket and pile elements, which is based on the force formulation (Spacone et al. 1996). In this model, the element is subdivided longitudinally into a number of segments, and the fibre discretisation approach has been employed to numerically model the cross section of each segment. The considered stress–strain relationship for the steel material of the pile and jacket members is based on the Menegotto-Pinto model (Menegotto and Pinto 1973). One of

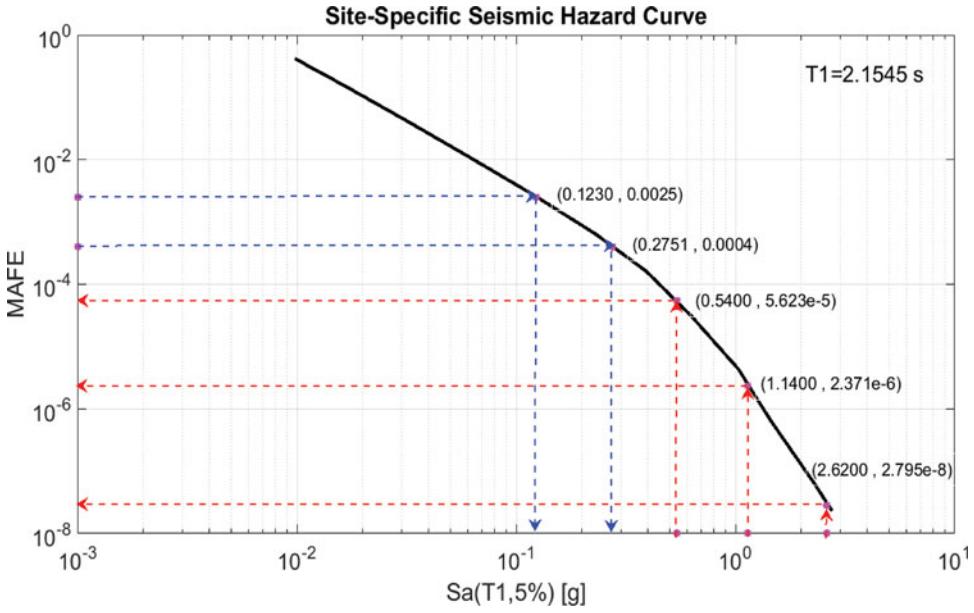

Figure 2. Site-specific seismic hazard curve for the fixed jacket platform located in Persian Gulf. (This figure is available in colour online.)

the merits of this type of material is the gradual transition from linear to nonlinear range of response. Moreover, the cyclic behaviour of this material is fairly consistent with experimental tests including Baushinger effects.

The nonlinear beam-column element used in this research is limited to small deformations in the basic system of the element. The large displacements are taken into consideration by embedding the basic system of the element in a corotational framework, as proposed by De Souza (Souza 2000). Also, the nonlinear geometry effects can be readily incorporated during the transformation of the basic response quantities to the global reference system of the structural model.

In order to include global buckling in the braces of JTOP, the brace is modelled with two force-based elements and an initial camber equal to 1/1000 of brace length on the mid node of the brace. Considering this technique along with co-rotational formulation for coordinate transformation, buckling and post-buckling behaviour of braces can be taken into consideration, accurately.

Asgarian et al. (2005) modelled the post buckling and also hysteretic behaviour of pinned and fixed tubular struts which were subjected to cyclic loading, using the force-based fibre beam column element. Asgarian et al. (2006) and Honarvar et al. (2008) used the same element in their studies to predict the seismic response of tested X-braced jackets. Furthermore, Alanjari et al. (2009) and Uriz et al. (2008) worked on the seismic performance of individual tubular strut tested by Black et al. (1980) upon buckling in compression as well as their capability in dissipating energy in consecutive cycles utilising the same element as the case here. All the aforementioned studies confirmed the efficiency of nonlinear beam column element for the steel jacket platform.

A beam on nonlinear Winkler foundation (BNWF) numerical model is created to perform uncoupled seismic soil-pile-superstructure interaction (SPSI) analysis. In order to model the pile elements in OpenSEES, nonlinear beam-column element is again employed. Zero length elements whose force-deformation constitutive behaviour representing soil near field springs are connected to every nodes of pile below the soil surface. Uniaxial *p-y* and *t-z* and *q-z* material objects in the lateral and vertical directions were assigned to these zero length elements. The PySimple1 uniaxial material model class in OpenSEES has been used to mimic the lateral behaviour of near-field soil. This element is formulated and verified with experimental data by Boulanger et al. (1999). The *t-z* materials were incorporated into zero length elements to apply skin friction on the pile, and a *q-z* element is also assigned under the pile to model the end bearing reaction.

Soil profile horizontal response should be derived as a function of depth to vertically propagating shear waves, as the first step of uncoupled SSPSI analysis. To model the saturated soil deposit dynamic response, a two-phase material based on Biot theory for porous media has been applied. In OpenSEES, four-node plane strain quadUp element implements a simplified numerical formulation of this theory known as U-P formulation. In addition, in order to simulate the stress–strain behaviour of the sand and bay mud, the pressure-dependent multi yield (Yang et al. 2003; Mazzoni et al. 2007) material and the pressure-independent multi yield (PIMY) material have been used, respectively. The procedure of conducting free field site response analysis and the soil-pile-structure interaction modelling approach implemented in this study has been verified with experimental data in a previous work of the authors (Asgarian et al. 2013).

Damping as presented by Equation (4) is referred to Rayleigh proportional damping (Charney 2008), which has been frequently used in previous studies (Asgarian and Ajamy 2010; Ajamy et al. 2014).

$$C = a_0.M + a_1.K \tag{4}$$

The first term of the aforementioned equation is the mass proportional term M and the second one is the stiffness proportional term K. Rayleigh damping is supposed to simulate the

Table 1. Seismic characteristics of the 40 ground motion records adopted for IDA (Baker et al. 2011).

REC No	NGA REC No	Earthquake name	Year	Station	*M*	*R* (km)	V_s30 (m/s)
1	72	San Fernando	1971	Lake Hughes #4	6.6	25.1	822
2	769	Loma Prieta	1989	Gilroy array #6	6.9	18.3	663
3	1165	Kocaeli, Turkey	1999	Izmit	7.5	7.2	811
4	1011	Northridge-01	1994	LA – Wonderland Ave	6.7	20.3	1223
5	164	Imperial Valley–06	1979	Cerro Prieto	6.5	15.2	660
6	1787	Hector Mine	1999	Hector	7.1	11.7	685
7	80	San Fernando	1971	Pasadena – Old Seismo Lab	6.6	21.5	969
8	1618	Duzce, Turkey	1999	Lamont 531	7.1	8.0	660
9	1786	Hector Mine	1999	Heart Bar state Park	7.1	61.2	685
10	1551	Chi-Chi, Taiwan	1999	TCU138	7.6	9.8	653
11	3507	Chi-Chi, Taiwan-06	1999	TCU129	6.3	24.8	664
12	150	Coyote Lake	1979	Gilroy array #6	5.7	3.1	663
13	572	Taiwan SMART1(45)	1986	SMART1 E02	7.3	-	660
14	285	Irpinia, Italy-01	1980	Bagnoli Irpinio	6.9	8.2	1000
15	801	Loma Prieta	1989	San Jose – Santa Teresa Hills	6.9	14.7	672
16	286	Irpinia, Italy-01	1980	Bisaccia	6.9	21.3	1000
17	1485	Chi-Chi, Taiwan	1999	TCU045	7.6	26.0	705
18	1161	Kocaeli, Turkey	1999	Gebze	7.5	10.9	792
19	1050	Northridge-01	1994	Pacomia Dam (downstr)	6.7	7.0	2016
20	2107	Denali, Alaska	2002	Carlo (temp)	7.9	50.9	964
21	1	Helena, Montana-01	1935	Carroll college	6.0	-	660
22	1091	Northridge–01	1994	Vasquez Rocks Park	6.7	23.6	996
23	1596	Chi-Chi, Taiwan	1999	WNT	7.6	1.8	664
24	771	Loma Prieta	1989	Golden Gate Bridge	6.9	79.8	642
25	809	Loma Prieta	1989	UCSC	6.9	18.5	714
26	265	Victoria, Mexico	1980	Cerro Prieto	6.3	14.4	660
27	1078	Northridge–01	1994	Santa Susana Ground	6.7	16.7	715
28	763	Loma Prieta	1989	Gilory – Gavilan Coll	6.9	10.0	730
29	1619	Duzce, Turkey	1999	Mudurnu	7.1	34.3	660
30	957	Northridge–01	1994	Burbank – Howard Rd.	6.7	16.9	822
31	2661	Chi-Chi, Taiwan-03	1999	TCU138	6.2	22.2	653
32	3509	Chi-Chi, Taiwan-06	1999	TCU138	6.3	33.6	653
33	810	Loma Prieta	1989	UCSC Lick Observation	6.9	18.4	714
34	765	Loma Prieta	1989	Gilory Array #1	6.9	9.6	1428
35	1013	Northridge–01	1994	LA Dam	6.7	5.9	629
36	1012	Northridge–01	1994	LA 00	6.7	19.1	706
37	1626	Sitka, Alaska	1972	Sitka Observatory	7.7	34.6	660
38	989	Northridge–01	1994	LA – Chalon Rd	6.7	20.5	740
39	748	Loma Prieta	1989	Belmont – Envirotech	6.9	44.1	628
40	1549	Chi-Chi, Taiwan	1999	TCU129	7.6	1.8	664

condition that the structure is submerged in a viscous fluid when the fluid imposes drag force on the structure .This is the reason of using Rayleigh damping in the numerical model of the offshore structures. a_0 and a_1 are the proportional coefficients which are determined by specifying the damping ratio in any two vibration modes (Charney 2008). It should be emphasised that when the system responds inelastically, the stiffness term indicated in Equation (4) changes. Hence, in order to deal with the inelastic response, the proportional coefficients a_0 and a_1 are computed on the basis of the initial stiffness, and the damping matrix is updated each time the tangent stiffness changes. In this case, the damping matrix will be classical at each step in the analysis as the current mode shapes will diagonalise the updated stiffness matrix (Charney 2008).

5. Record selection and site specific seismic hazard curve

In this investigation, a suite of 40 unscaled three-component far field ground motion records are selected so that their horizontal response spectra fairly match the target mean and standard deviations in full logarithmic coordinates predicted for a magnitude of 7 strike-slip earthquake at a distance of 10 km (Baker et al. 2011). The target response spectrum represents the high-seismicity sites that may experience strong ground motions from mid to large-magnitude earthquakes at close distances. The ground motions were selected to match this target at periods between 0 and 5 sec. The site Vs30 (average shear wave velocity in the top 30 m) was assumed to be 750 m/s representing a rock site, which is supposed to be used as bedrock level ground motions for site response analysis (Baker et al. 2011). Since the ground motion set is neither structure-specific nor site-specific, the selected records have a variety of spectral shapes over a wide range of periods, and are capable of modelling the aleatoric uncertainties in the structural analyses. The seismic characteristics of the 40 selected ground motions are tabulated in Table 1.

Further, the site-specific probabilistic seismic hazard curve that corresponds to the fundamental period of the structure (T1 = 2.15 s) has been calculated by probabilistic seismic hazard analysis (PSHA) (Bazzurro and Cornell 1999), and plotted in Figure 2. The corresponding S_a for each value of mean annual frequency of exceedance can be obtained from this figure.

6. Results and discussions

As the first result presentation, the IDA curves as well as the sample median and the sample geometric mean of the NC demand responses and the points associated with global

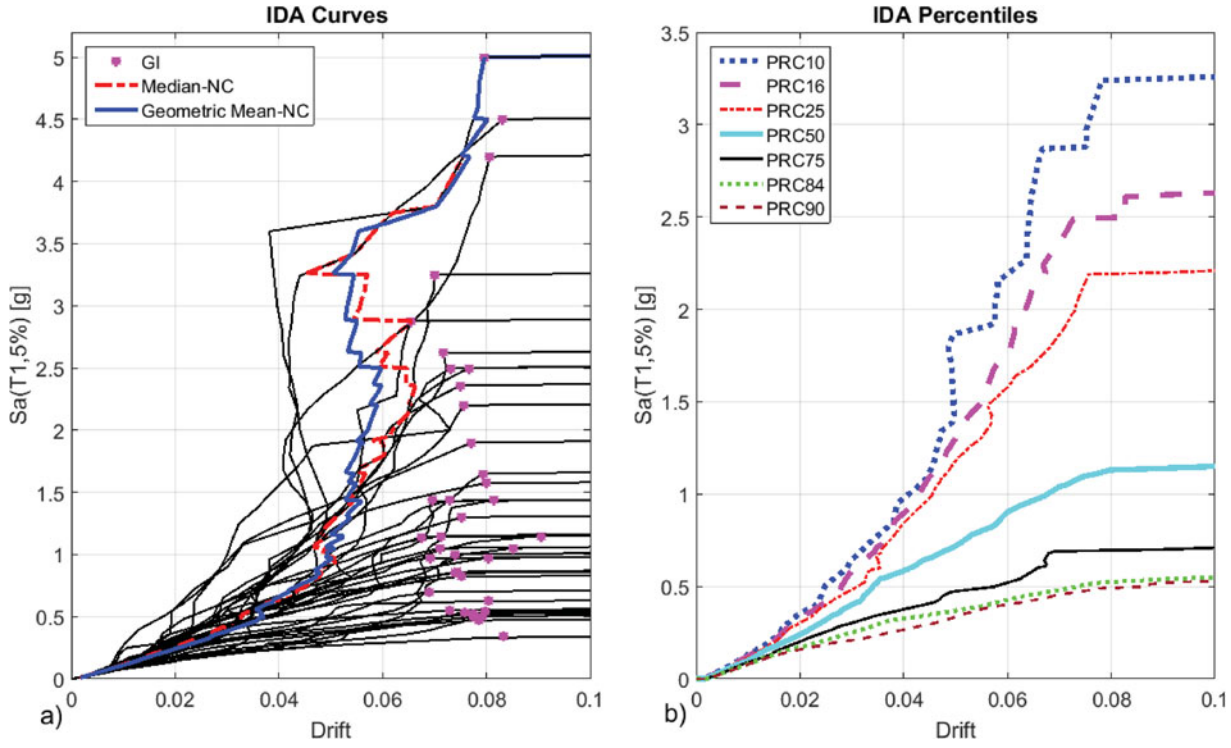

Figure 3. (a) IDA curves, sample median and sample geometric mean of non-collapse records and the GI limit state and (b) summarised IDA curves (10%, 16%, 25%, 50%, 75%, 84% and 90% percentiles). (This figure is available in colour online.)

instability (GI) limit state (where the IDA curves flatten) have been all illustrated in Figure 3(a). In addition to this, the summarised IDA curves (10%, 16%, 25%, 50%, 75%, 84% and 90% percentiles) are depicted in Figure 3(b). Since, in this study the failure mode of the numerical model – in most of the nonlinear analyses – is the portal frame mechanism in piles, the pile drift per unit length of the pile has been considered as the EDP. Moreover, the 5% damped elastic spectral acceleration at the fundamental period of the structure (S_a(T1,5%)) has been chosen as the IM.

As is seen, the sample median and the sample geometric mean of the NC demand responses are significantly different,

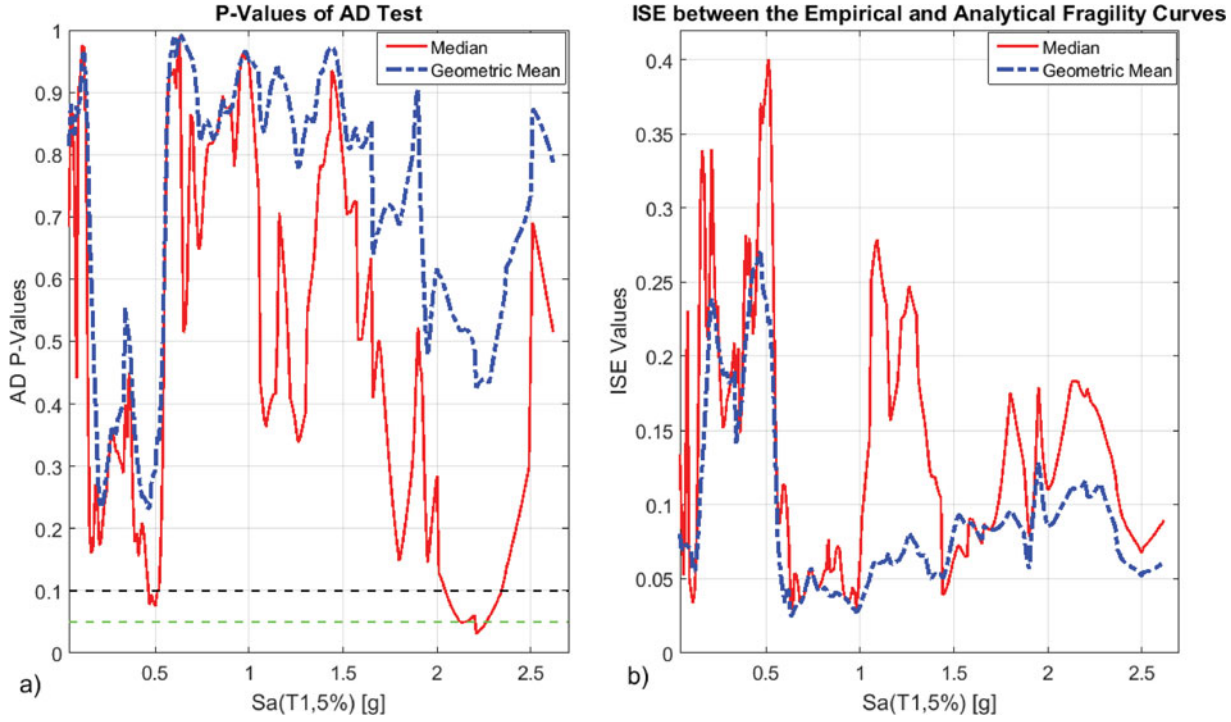

Figure 4. (a) AD P-values based on the sample median and sample geometric mean and (b) ISE values based on the sample median and sample geometric mean. (This figure is available in colour online.)

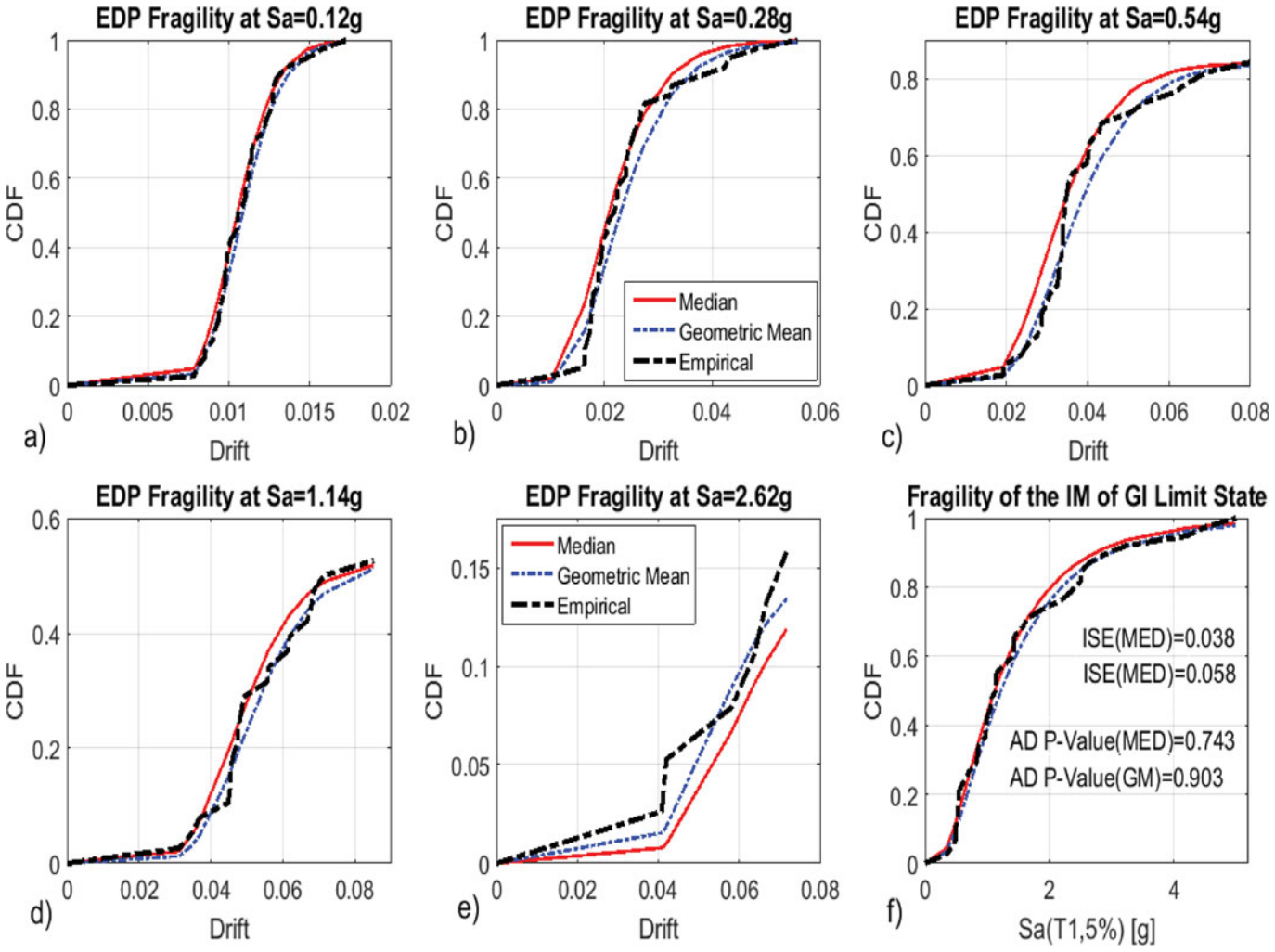

Figure 5. Empirical and analytical seismic fragility curves of drift demand at (a) $S_a = 0.12g$, (b) $S_a = 0.28g$, (c) $S_a = 0.54g$, (d) $S_a = 1.14g$, (e) $S_a = 2.62g$and (f) empirical and analytical seismic fragility curves of the IM of GI limit state. (This figure is available in colour online.)

especially at the IM levels where several records have reached their GI limit state. Therefore, considering either of them as the estimator of lognormal central tendency could point to different results in seismic fragility assessment of the sample platform.

Prior to obtaining the seismic fragility curves, it is intended to investigate the validity of the lognormal hypothesise for the drift demand at each IM level. To this purpose, AD goodness of fit test (Anderson and Darling 1954) has been employed. In fact, the lognormal hypothesise for the drift demand at each IM level is rejected if the AD *P*-value is less than the probability of Type 1 error which is referred to as the significance level α(Anderson and Darling 1954; Soong 2004). Commonly α is equal to 0.01, 0.05 or 0.10 (Soong 2004), and in this study it is assumed that $\alpha = 0.05, 0.10$. Regarding both the sample median and the sample geometric mean as the lognormal central tendency, the AD P-values of the drift demand at each IM level are illustrated in Figure 4(a).

It is evident from the figure that the AD *P*-values based on the sample geometric mean are greater than the AD *P*-values based on the sample median at all the IM levels, which indicates that the lognormal hypothesise is rejected at higher significance levels if the sample geometric mean is considered as the statistical estimator of lognormal central tendency. Moreover, it is observed that for $\alpha = 0.10$, the lognormal assumption is not accepted at several IM levels where the AD P-values are less than 0.10 (the black dashed line) if the sample median is supposed to be the estimator of central tendency. Even in case $\alpha = 0.05$ (the green dashed line), there are still a few IM levels around $S_a = 2.2g$ where the lognormal assumption is rejected based on the sample median.

In the next step, the analytical seismic fragility curves of drift demand based on both the sample median and the sample geometric mean as well as the empirical fragility curves have been assessed for two IM levels (0.1230 and 0.2751 g) corresponding to the 400 and 2500 year return period earthquakes as recommended by API RP2A-WSD (2007). In addition, the seismic fragility of drift demand have been computed for the IM levels at which 16%, 50% and 84% ground motion records reach their global dynamic instability limit states. These IM levels (0.54, 1.14 and 2.62) correspond to the 17,783, 421,696 and 35,774,322 year return period earthquakes, respectively (see Figure 2). Also, the analytical and empirical fragilities of collapse limit state (the IM values associated with onset of GI limit state) have been calculated for the sample platform. All the aforementioned seismic fragility curves are demonstrated in Figure 5.

It is emphasised that the lognormal assumption is accepted for all the IM levels at which the analytical seismic fragility curves are presented in Figure 5. As is observed, the fragility curves do not reach unity at the IM levels equal to 0.54, 1.14 and 2.62 g as several ground motion records have reached their collapse capacities at these IM levels. As described in Section 2.2, $P_{NC|S_a}$ is equal to unity if no record has reached the GI limit state. Otherwise, the term $P_{NC|S_a}$ is definitely less than unity and so does the maximum value of the fragility function. Additionally, it can be seen that the analytical fragility functions based on the sample geometric are closer to the empirical fragility functions. In order to verify such observation with a quantitative criterion, the integrated squared error (ISE) – known as L_2 distance – (Clarke et al. 2012) between the lognormal CDF and the ECDF of the drift demand based on the sample median and the sample geometric mean (at all the IM levels) have been assessed by Equations (5) and (6) using the composite Gauss–Legendre integration technique (Hildebrand 1956), and shown in Figure 4(b).

$$\mathrm{ISE}_{[\eta]} = \int_{-\infty}^{+\infty} \left[\mathrm{ECDF}(x) - \mathrm{CDF}_{[\eta]}(x)\right]^2 .dx \qquad (5)$$

$$\mathrm{ISE}_{[\mathrm{GM}]} = \int_{-\infty}^{+\infty} \left[\mathrm{ECDF}(x) - \mathrm{CDF}_{[\mathrm{GM}]}(x)\right]^2 .dx \qquad (6)$$

The indices $[\eta]$ and $[GM]$ following each parameter refer to calculation of that parameter based on the sample median and the sample geometric mean, and the variable x is referred to different levels of the MIDR demand.

Figure 4(b) reveals that the ISE values based on the sample geometric mean are less than the ISE values based on the sample median at most of the IM levels, which could be considered as other evidence for the sample geometric mean or against the sample median. Analogously, the ISE value of the IM of GI limit state based on the sample geometric mean is less than the one based on the sample median (these values are illustrated on Figure 5(f)).

7. Conclusions

In this paper, the validity of lognormal distribution of the drift demand and spectral acceleration capacity for the JTOPs has been investigated by the powerful AD goodness of fit test. In this regard, both the sample median and the sample geometric mean have been considered as the estimator of lognormal central tendency. All the conclusions are drawn as follows:

- The lognormal hypothesise of the spectral accelerations associated with onset of collapse and the drift demand at all the IM levels for the sample offshore platform is accepted by the AD goodness of fit test if the sample geometric mean is considered as the lognormal central tendency. On the contrary, lognormal assumption based on the sample median as the index of central tendency can be rejected for the sample jacket platform at some IM levels.
- The discrepancies between the sample median and the sample geometric mean of the NC drift demands grow as the IM value increases. The reason is that the records reach their GI limit states at higher IM levels.
- The AD P-values of the drift demand of the sample offshore platform based on the sample geometric mean are greater than the AD P-values based on the sample median at all the IM levels. This could be considered as substantial evidence for the sample geometric mean and against the sample median.
- The AD P-value of the spectral accelerations associated with the onset of collapse based on the sample geometric mean is again greater than the one based on the sample median.
- The ISE values between the empirical and analytical fragility of the drift demand of the jacket platform based on the sample geometric mean are less than the ones based on the sample median at most of the IM levels.

Disclosure statement

No potential conflict of interest was reported by the authors.

References

Abyani M, Asgarian B, Zarrin M. Forthcoming 2017. Sample geometric mean versus sample median in closed form framework of seismic reliability evaluation: a case study comparison. Earthq Eng Eng Vib.

AISC. 2003. LRFD Manual of steel construction. 3rd ed. Chicago (IL): American Institute of Steel Construction.

Ajamy A, Zolfaghari MR, Asgarian B, Ventura CE. 2014. Probabilistic seismic analysis of offshore platforms incorporating uncertainty in soil-pile-structure interactions. J Constr Steel Res. 101:265–279.

Alanjari P, Asgarian B, Bahaari MR, Honarvar MR. 2009. On the energy dissipation of jacket type offshore platforms with different pile–leg interactions. Appl Ocean Res. 31(2):82–89.

Anderson TW, Darling DA. 1954. A test of goodness-of-fit. J Am Statist Assoc. 49:765–769.

API RP2A-WSD. 2007. American Petroleum Institute recommended practice for planning, designing and constructing fixed offshore platforms. 21st ed. Washington (DC).

Asgarian B, Aghakouchak AA, Bea RG. 2005. Inelastic post buckling and cyclic behavior of tubular braces. ASME J Offshore Mech Arct Eng. 127(3):256–262.

Asgarian B, Aghakouchack AA, Bea RG. 2006. Non-linear analysis of jacket type offshore platforms using fiber elements. Offshore Mech Arct Eng. 128(3):224–232.

Asgarian B, Ajamy A. 2010. Seismic performance of jacket type offshore platforms through incremental dynamic analysis. Offshore Mech Arct Eng. 132(3):1–14.

Asgarian B, Zarrin M, Boroumand M. 2013. Nonlinear dynamic analysis of pile foundation subjected to strong ground motion using fiber elements. Int J Marit Technol. 1(1):35–46.

Baker JW, Shahi SK, Jayaram N. 2011. New ground motion selection procedures and selected motions for the peer transportation research program. Berkeley (CA): Pacific Earthquake Engineering Research Center, University of California. PEER Report.

Bazzurro P, Cornell CA. 1999. Disaggregation of seismic hazard. Bull Seismol Soc Am. 81:501–509.

Benjamin JR, Cornell CA. 1970. Probability, statistics and decision for civil engineers. New York (NY): McGraw-Hill.

Black RG, Wenger WAB, Popov EP. 1980. Inelastic buckling of steel strut under cyclic load reversals. Berkeley (CA): Earthquake Engineering Research Center. Univ. of California. Report No. UCB/EERC-80/40.

Boulanger RW, Curras C1, Kutter BL, Wilson DW, Abghari A. 1999. Seismic soil-pile-structure interaction experiments and analyses, J Geotech Geoenviron Eng. 125(9):750–759.

Celik OC, Ellingwood BR. 2010. Seismic fragilities for non-ductile reinforced concrete frames – role of aleatoric and epistemic uncertainties. Struct Saf. 32(1):1–12.

Charney FA. 2008. Unintended consequences of modeling damping in structures. J Struct Eng. 134(4):581–592.

Clarke BR, McKinnon PL, Riley G. 2012. A fast robust method for fitting gamma distributions. Statistical Papers. 53:1001–1014.
Cornell CA, Jalayer F, Hamburger R, Foutch D. 2002. Probabilistic basis for 2000 SAC Federal Emergency Management Agency steel moment frame guidelines. J Struct Eng. 128(4):526–533.
De Souza R. 2000. Forced-based finite element for large displacement inelastic analysis of frames [PhD thesis]. Berkeley (CA): University of California.
DNV. 1996. Guideline for offshore structural reliability analysis: examples for jacket platforms. Hovik: Det Norske Veritas.
El-Din MN, Kim J. 2014. Simplified seismic life cycle cost estimation of a steel jacket offshore platform structure. Struct Infrastruct Eng. 13(8):1027–1044.
Elsayed T, El-Shaib M, Gbr k. 2016. Reliability of fixed offshore jacket platform against earthquake collapse. J Ships Offshore Struct. 11(2):167–181.
Engmann S, Cousineau D. 2011. Comparing distributions: the two-sample Anderson-Darling test as an alternative to the Kolmogorov-Smirnoff test. J Appl Quant Methods. 6:1–17.
Golafshani AA, Ebrahimian H, Bagheri V, Holmas T. 2011. Assessment of offshore platforms under extreme waves by probabilistic incremental wave analysis. J Constr Steel Res. 67(5):759–769.
Hasan SD, Islam N, Moin K. 2010. A review of fixed offshore platforms under earthquake forces. Struct Eng Mech. 35(4):479–491.
Hildebrand FB. 1956. Introduction to numerical analysis. New York (NY): McGraw-Hill
Honarvar MR, Bahari MR, Asgarian B, Alanjari P. 2008. Cyclic inelastic behavior and analytical modeling of pile leg interaction in jacket type offshore platform. Appl Ocean Res. 29(4):167–179.
Jahanmard V, Dastan MA, Mehdigholi H, Tabeshpour MR, Seif MS. 2015. Performance-based assessment of steel jacket platforms by wave endurance time method. J Ships Offshore Struct. 12(1):32–42.
Jalayer F. 2003. Direct probabilistic seismic analysis: implementing nonlinear dynamic assessments [PhD thesis]. Stanford (CA): Department of Civil and Environmental Engineering, Stanford University.
Mazzoni S, McKenna F, Scott M, Fenves G. 2007. Open system for earthquake engineering simulation (OpenSEES) - OpenSEES command language manual. Berkeley (CA): University of California.
McKay MD, Beckman RJ, Conover WJ. 1979. A comparison of three methods for selecting values of input variables in the analysis of output from a computer code. Technometrics. 21(2):239–245.
Menegotto M, Pinto P. 1973. Method of analysis for cyclically loaded reinforced concrete plane frame including changes in geometry and non-elastic behavior of elements under combined normal force and bending, Proceeding, IABSE symposium on resistance and ultimate deformability of structures acted on by well defined repeated loads. International Association of Bridge and Structural Engineering, Libson, Portugal. 13:15–22.
Razali NM, Wah YB. 2011. Power comparison of Shapiro-wilk, Kolmogrov Smirnov, Lillefors and Anderson Darling tests. J Stat Model Analytics. 2(1):21–33.
SAC/FEMA. 2000a. Recommended seismic design criteria for new steel moment frame buildings. Washington (DC): SAC Joint Venture, Federal Emergency Management Agency. Report No. FEMA-350.
SAC/FEMA. 2000b. Recommended seismic evaluation and upgrade criteria for existing welded steel moment-frame buildings. Washington (DC): Federal Emergency Management Agency. Report No. FEMA-351,
Shih WJ, Binkowitz B. 1967. Median versus geometric mean for lognormal samples. J Statist Comput Simulation. 28(1):81–83.
Shome N. 1999. Probabilistic seismic demand analysis of nonlinear structures [PhD thesis]. Stanford (CA): Department of Civil and Environmental Engineering.
Soong TT. 2004. Fundamentals of probability and statistics for engineers. Buffalo (NY): State University of New York at Buffalo.
Spacone E, Filippou FC, Taucer FF. 1996. Fiber beamcolumn model for nonlinear analysis of RC frames. I: Formulation. Earthquake Eng Struct Dyn. 25(7):711–725.
Uriz P, Filippou FC, Mahin SA. 2008. Model for cyclic inelastic buckling of steel braces. Struct Eng. 134(4):619–628.
Vamvatsikos D, Cornell CA. 2002. Incremental dynamic analysis. Earthquake Eng Struct Dyn. 31(3):491–514.
Vamvatsikos D. 2013. Derivation of new SAC/FEMA performance evaluation solutions with second-order hazard approximation. Earthquake Eng Struct Dyn. 42(8):1171–1188.
Vorechovsky M, Novak D. 2009. Correlation control in small-sample Monte Carlo type simulations 1: a simulated annealing approach. Probab Eng Mech. 24:452–462.
Walpole RE, Myers RH, Myers SL, Ye K. 2002. Probability and statistics for engineers and scientists.
Yang Z, Elgamal A, Parra E. (2003). Computational model for cyclic mobility and associated shear deformation. J Geotech Geoenviron Eng. 129(12):1119–1127.